Check for updates

Received: 23 March 2026 | Revised: 22 June 2026 | Accepted: 1 July 2026

DOI: 10.1002/inf2.70170

RESEARCH ARTICLE

WILEY

Building a library of electrocatalysts based on single-centered metallophthalocyanines

Jin Hyuk Cho[1] | **Yong Hyun Moon**[2] | **Gwonho Yu**[3] | **Moon Sung Kang**[4] | **Ji Hee Jang**[2] | **Heesung Yoon**[1] | **Jaehyun Kim**[5] | **Ho Won Jang**[5] | **Sang Hyun Ahn**[6] | **Seoin Back**[3,7] | **Youn Jeong Jang**[2] | **Soo Young Kim**[1]

[1]Department of Materials Science and Engineering, Korea University, Seoul, Republic of Korea

[2]Department of Chemical Engineering, Hanyang University, Seoul, Republic of Korea

[3]KU-KIST Graduate School of Converging Science and Technology, Korea University, Seoul, Republic of Korea

[4]Department of Cogno-Mechatronics Engineering, College of Nanoscience and Nanotechnology, Pusan National University, Busan, Republic of Korea

[5]Department of Materials Science and Engineering, Seoul National University, Seoul, Republic of Korea

[6]Department of Chemical Engineering, Chung-Ang University, Seoul, Republic of Korea

[7]Department of Integrative Energy Engineering, Korea University, Seoul, Republic of Korea

Correspondence

Seoin Back, KU-KIST Graduate School of Converging Science and Technology, Korea University, Seoul 02841, Republic of Korea.
Email: sback@korea.ac.kr

Youn Jeong Jang, Department of Chemical Engineering, Hanyang University, Seoul 04763, Republic of Korea.
Email: yjang53@hanyang.ac.kr

Soo Young Kim, Department of Materials Science and Engineering, Korea University, Seoul 02841, Republic of Korea.
Email: sooyoungkim@korea.ac.kr

Funding information

National Research Foundation of Korea, Grant/Award Numbers: RS-2025-00558945, RS-2025-02214715

Abstract

Technologies for electrochemical energy conversion play a pivotal role in mitigating global warming and facilitating the transition to a sustainable energy society. Metallophthalocyanine-based electrocatalysts offer significant advantages due to their coordination flexibility, tunability, and electron-deficient nature, all of which enhance electron transfer. Herein, we present a systematically designed electrocatalyst library comprising eight metallophthalocyanines, each tailored to address five key energy conversion reactions. By integrating theoretical modeling with experimental approaches, we conduct an in-depth analysis of the electronic configurations and atomic symmetries of the catalysts. Our study elucidates not only the intrinsic catalytic efficiency but also the scalable synthesis and practical deployability of these electrocatalysts, thereby substantiating their potential for real-world applications. Overall, we aim to accelerate the energy transition, reduce environmental impact, and enhance economic competitiveness by establishing a robust electrocatalyst library for a carbon circular economy.

KEYWORDS

carbon neutrality, electrocatalysts, energy conversion, metallophthalocyanines

Jin Hyuk Cho, Yong Hyun Moon, and Gwonho Yu contributed equally to this work.

This is an open access article under the terms of the Creative Commons Attribution License, which permits use, distribution and reproduction in any medium, provided the original work is properly cited.

© 2026 The Author(s). *InfoMat* published by UESTC and John Wiley & Sons Australia, Ltd.

1 | INTRODUCTION

The depletion of fossil fuel reserves and the substantial CO_2 emissions generated from their combustion pose critical threats to human civilization.[1–3] As a result, sustainable and renewable energy sources are increasingly being recognized as viable solutions.[4] The market valuation of this sector is projected to grow from USD 1.34 trillion in 2024 to USD 5.62 trillion by 2033, reflecting a compound annual growth rate (CAGR) of approximately 17.3%. This rapid expansion has spurred significant investments at both industrial and national levels, highlighting the pivotal role of the sector in the global energy transition. Electrochemical energy conversion, a transformative technology that facilitates the interconversion of electrical and chemical energy via electron and ion transport, has emerged as a key strategy for achieving carbon neutrality.[5,6] At the forefront of this field are fundamental electrochemical reactions, including the hydrogen evolution reaction (HER),[7] carbon dioxide reduction reaction (CO_2RR),[8] nitrogen reduction reaction (NRR),[9] oxygen evolution reaction (OER),[10] and oxygen reduction reaction (ORR)[11]—all of which are instrumental in advancing sustainable energy technologies. However, unlocking the full potential of these processes necessitates the development of high-performance electrocatalysts with enhanced activity, selectivity, stability, and cost-effectiveness.[12] Such advancements are critical for overcoming existing technological barriers and accelerating the transition toward sustainable energy solutions.

Metallophthalocyanine (MPc) is a tetrapyrrole-based coordination complex in which four nitrogen atoms coordinate with a central metal ion, conferring remarkable stability and robustness.[10,13] This molecular architecture is widely utilized as an electrocatalyst due to its highly π-conjugated framework, which augments chemical stability and facilitates efficient electron transport.[14,15] Additionally, the incorporation of various central metal ions modulates the physicochemical properties of MPc, allowing for tailored applications depending on the specific metal center.[16,17] To further improve catalytic activity and cost-effectiveness, ongoing research explores the immobilization of MPc onto different support materials, as these interactions can significantly enhance catalytic efficiency by optimizing dispersion and electronic properties. In particular, single-walled and multi-walled carbon nanotubes (CNTs) are considered exemplary support materials due to their ability to uniformly distribute metal complexes across their surfaces, thereby mitigating aggregation.[14–19] Furthermore, their exceptional mechanical strength, coupled with their intrinsically high electrical conductivity, contributes to a substantial improvement in catalytic activity.[15]

Herein, we report a one-step solution-based synthesis approach that eliminates the need for additional processing. This approach enables the uniform dispersion of precisely controlled loadings of eight different MPc species onto multi-walled CNTs, denoted as MPc-CNTs (M = Fe, Co, Ni, Cu, Zn, Mn, Sn, and Pb (Pd)). The structural and compositional characteristics of the synthesized electrocatalysts were confirmed using multiple characterization techniques, and theoretical modeling further validated these features. Subsequently, the fabricated catalysts were evaluated for their performance in five distinct electrochemical energy-conversion reactions: CO_2RR, HER, NRR, OER, and ORR.

In CO_2RR, CoPc-CNT, NiPc-CNT, and FePc-CNT have demonstrated exceptional Faradaic efficiencies (FE) in converting CO_2 to CO, achieving nearly 100% FE_{CO}. Additionally, these catalysts exhibited a remarkable 798.53-fold enhancement in CO_2RR price-activity relative to commercial Ag foil at −0.8 V versus reversible hydrogen electrode (RHE). Notably, CoPc-CNT displayed outstanding catalytic performance when incorporated into a membrane electrode assembly (MEA) specifically designed to minimize ohmic losses, successfully maintaining an FE_{CO} of 99.2% at 200 mA cm^{-2}. Both FePc-CNT and CoPc-CNT showed significantly improved hydrogen (H_2) evolution activity compared to pristine CNTs. This enhancement was reflected in their low Tafel slopes of 141 and 119 mV dec^{-1}, respectively, as well as their overpotentials of 355 and 393 mV at a current density of 10 mA cm^{-2}. Moreover, by employing an alkaline medium in a large-scale practical anion exchange membrane water electrolyzer (AEMWE) operated at 80°C, CoPc-CNT achieved an impressive ampere-level current density of 2 A cm^{-2} at 2.5 V (bias current: 10 A, electrode area: 5 cm^2). For ammonia (NH_3) synthesis through NRR, NiPc-CNT exhibited outstanding performance, achieving an FE of 18.1%, a production rate of 33.4 μg h^{-1} cm^{-2}, and stable operation for 8 h. In addition to its extraordinary NH_3 production rate (35.4 μg h^{-1} cm^{-2}), MnPc-CNT achieved an exceptional turnover frequency (TOF) of 14.9 h^{-1}, emphasizing its high intrinsic catalytic efficiency and accelerated kinetics. We further evaluated the catalytic activity of the eight MPc-CNT variants in the OER, focusing on their OER activity and overpotentials, as well as in the ORR, highlighting their half-wave potentials. In conclusion, we established a comprehensive library of MPc-based electrocatalysts for energy conversion applications, optimizing their performance through strategic selection for specific reactions and providing a foundation for their scalable development and practical industrial implementation.

25673165, 2026, 10, Downloaded from https://onlinelibrary.wiley.com/doi/10.1002/inf2.70170 by Hanyang University Library, Wiley Online Library on [08/11/2026]. See the Terms and Conditions (https://onlinelibrary.wiley.com/terms-and-conditions) on Wiley Online Library for rules of use; OA articles are governed by the applicable Creative Commons License

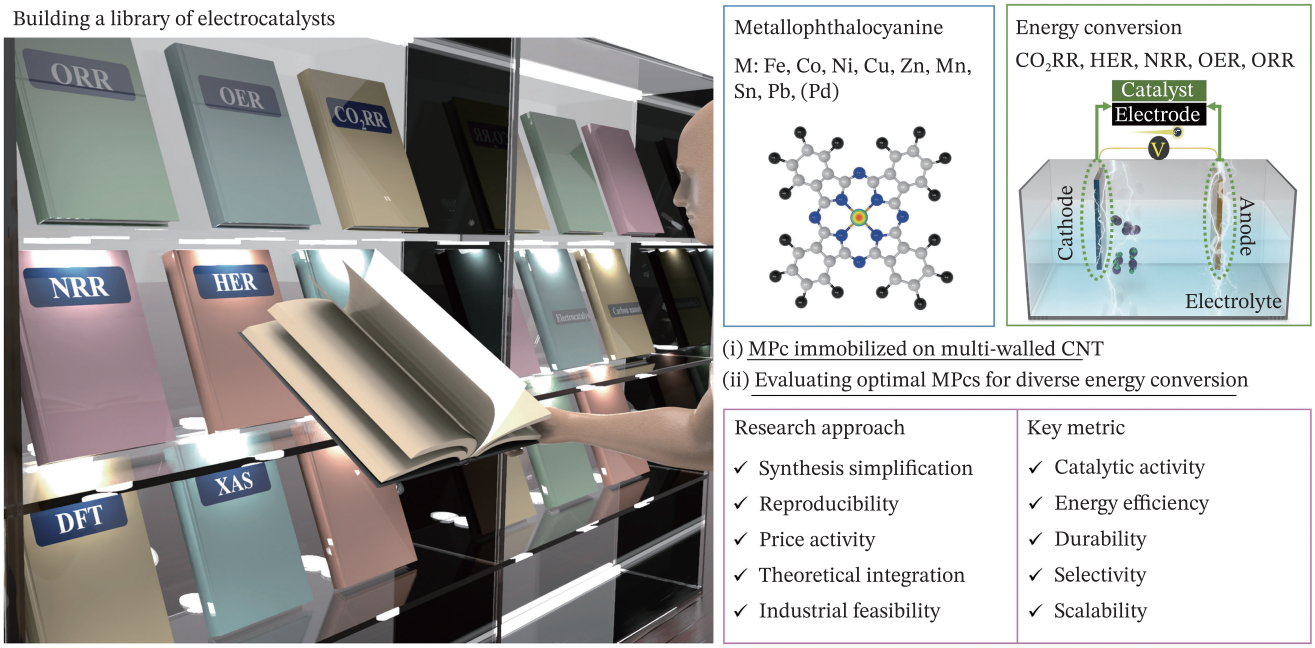

FIGURE 1 Strategies for ensuring a minimal environmental footprint and long-term ecological benefits through the construction of an extensive electrocatalyst library for next-generation energy conversion processes.

2 | RESULTS AND DISCUSSION

2.1 | Synthesis and characterization of eight types of MPc-CNTs

To identify the most efficient catalyst for five distinct energy conversion applications, eight MPc species were immobilized onto CNTs. The research approach encompasses the optimization of synthesis protocols, improvement of reproducibility, assessment of electrode price–activity, theoretical investigation, and evaluation of industrial feasibility (Figure 1). A comprehensive electrocatalytic characterization was performed to assess catalytic activity, energy efficiency, durability, selectivity, and scalability.

First, we selected eight MPc types based on their high compatibility and cost-effectiveness (Table S1). The MPcs and multi-walled CNTs were uniformly dispersed in *N*,*N*-dimethylformamide, followed by a one-step solution-phase synthesis under magnetic stirring, eliminating the need for additional processing steps (detailed synthesis procedures are provided in the Materials section of the Supporting Information). During synthesis, MPc molecules were partially anchored onto the carbon framework, facilitated by strong π–π interactions between the phthalocyanine ring and CNTs.

To ensure uniform distribution and maximize molecular efficiency, we carefully optimized the metal content to 0.8–2 wt%, as confirmed by inductively coupled plasma mass spectrometry (ICP-MS) (Table S2). Scanning electron microscopy (SEM) and high-resolution transmission electron microscopy (TEM) analyses confirmed the absence of MPc aggregation across all eight catalysts (Figures S1 and S2). The TEM images revealed no morphological changes or structural distortions. Simultaneously, TEM-energy dispersive X-ray spectroscopy (EDS) confirmed the presence of each metal element, supporting the molecular-level dispersion of MPc species on the CNT surface. This finding aligns with the powder X-ray diffraction (PXRD) results, which showed only the characteristic diffraction pattern of CNT, with no detectable MPc clusters (Figures S3 and S4). Moreover, as depicted in Figure $2A_1$–H_1, aberration-corrected high-angle annular dark-field scanning transmission electron microscopy (AC HAADF-STEM) images substantiate the homogeneous dispersion of isolated metallophthalocyanine molecules (bright dots) on the CNT sidewalls. Consistently, 3D Gaussian-fitting-based atomic overlap mapping further corroborates the atom-level dispersion of metal species in MPc-CNTs (Figures S5–S12). Next, X-ray photoelectron spectroscopy (XPS) was performed to investigate the electronic structure and surface composition of the individual MPc-CNT materials (Figure S13). The oxidation states of the metal centers in MPc-CNTs were estimated to fall within the range $M^{+} < M^{\delta} \leq M^{2+}$ (where M represents the metals), with no detectable metallic state, reinforcing the uniform distribution of MPc on the CNT surface. A detailed explanation of the

25673165, 2026, 10, Downloaded from https://onlinelibrary.wiley.com/doi/10.1002/inf2.70170 by Hanyang University Library, Wiley Online Library on [08/11/2026]. See the Terms and Conditions (https://onlinelibrary.wiley.com/terms-and-conditions) on Wiley Online Library for rules of use; OA articles are governed by the applicable Creative Commons License

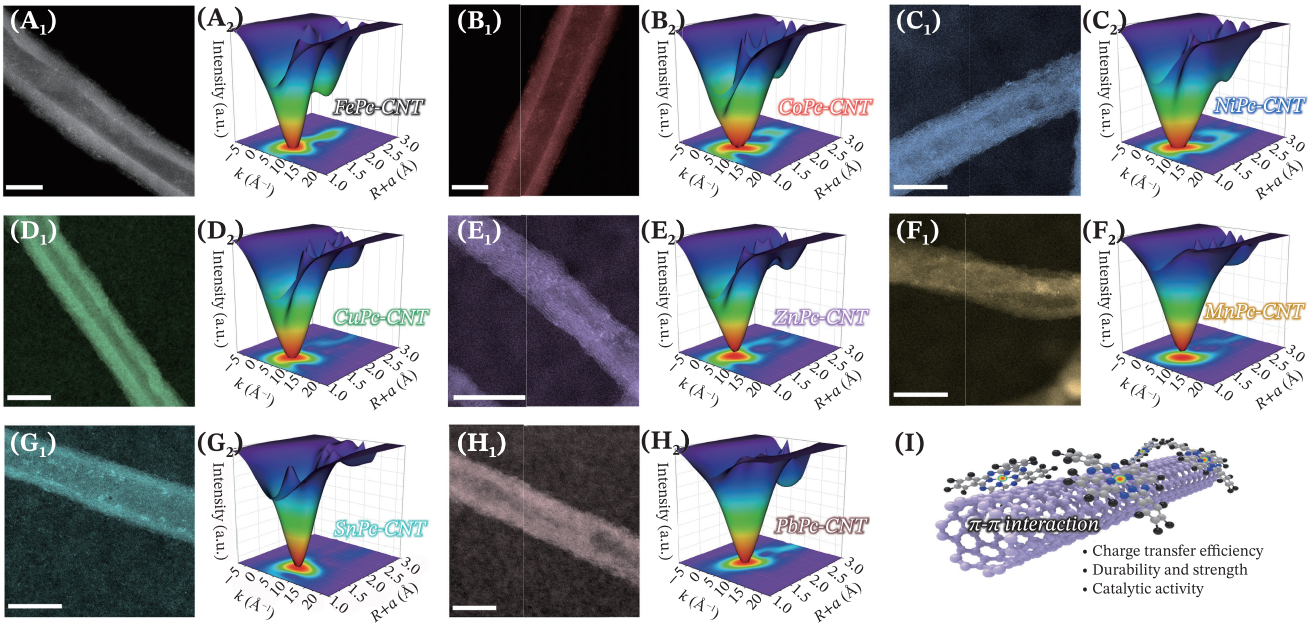

FIGURE 2 Atomic-level structural characterization of MPc-CNTs. AC HAADF-STEM images of (A_1) FePc-CNT, (B_1) CoPc-CNT, (C_1) NiPc-CNT, (D_1) CuPc-CNT, (E_1) ZnPc-CNT, (F_1) MnPc-CNT, (G_1) SnPc-CNT, and (H_1) PbPc-CNT (scale bar, 10 nm). To precisely elucidate the atomic environment of MPc-CNTs, both vertical and flat EXAFS 3D spectra are presented. Wavelet transform contour plots of the k^3-weighted FT-EXAFS data are shown for (A_2) FePc-CNT (Fe *K*-edge signal), (B_2) CoPc-CNT (Co *K*-edge signal), (C_2) NiPc-CNT (Ni *K*-edge signal), (D_2) CuPc-CNT (Cu *K*-edge signal), (E_2) ZnPc-CNT (Zn *K*-edge signal), (F_2) MnPc-CNT (Mn *K*-edge signal), (G_2) SnPc-CNT (Sn *K*-edge signal), and (H_2) PbPc-CNT (Pb L_3-edge signal). Additionally, (I) a conceptual schematic illustrates the MPc-CNT structure and the augmented physicochemical properties that arise from π-π interactions between MPc and CNT.

XPS analysis of MPc-CNTs is provided in Supporting Information Note 1. To further explore the intrinsic properties of the material, we employed X-ray absorption near-edge structure (XANES) spectroscopy—an advanced technique for probing electronic states and local structures. The valence states of MPc-CNTs were determined from the pre-edge features in the XANES spectra (Figure S14), which correspond to the $1s \rightarrow 3d$ quadrupole transitions and dipole-allowed transitions arising from the hybridization of 3d and 4p orbitals. To improve the reliability of the oxidation-state evaluation, we additionally analyzed the first-derivative XANES spectra, which accentuate slight edge shifts that are not readily observable in the normalized profiles (Figure S15). These results were subsequently compared with those of MPcs and metal foils. As a result, the oxidation state of MPc-CNTs was confirmed to fall within the range $M^{1+} < M^{\delta} \leq M^{2+}$. The $1s \rightarrow 4p$ transition peak in XANES spectra indicates that most MPc molecules adopt a stable square-planar symmetry (D_{4h}).[20] However, the larger ionic radii of Pb and Sn induce a non-planar distortion in PbPc and SnPc, resulting in a C_{4v}-type geometry that deviates from the ideal square planar arrangement observed in other MPcs. The atomic configuration of the MPc-CNTs was further examined using extended X-ray absorption fine structure (EXAFS). No evidence of M-M (metal–metal) bonding was detected at the metal edges of MPc–CNTs, and M–N (metal-nitrogen) bonds were distinctly observed in the first coordination shell, confirming the absence of MPc aggregation (Figure S16). Furthermore, consistent with the XANES data, peak shifts in the EXAFS results indicate that SnPc-CNT and PbPc-CNT exhibit elongated M–N bond distances (Table S3). This elongation is attributed to their inherent C_{4v} symmetry. Wavelet transform (WT)-EXAFS, which integrates *k*-space (representing the frequency domain) and *R*-space (representing real space), further validated M–N bonding and interatomic distances in MPc-CNTs (Figure 2A_2–H_2). The synergistic effect of molecularly dispersed MPc and CNT, along with associated advantages, is illustrated in the schematic shown in Figure 2I. To elucidate the structural and electronic properties of the MPc-based electrocatalysts, a series of density functional theory (DFT) analyses were performed. Since CNTs with diameters greater than a few nanometers exhibit negligible curvature effects, their properties closely resemble those of graphene.[21] Accordingly, a graphene model was employed to simulate the CNT support. The optimized distances between MPc molecules and the graphene surface ranged from 3.4 to 3.5 Å for all

25673165, 2026, 10, Downloaded from https://onlinelibrary.wiley.com/doi/10.1002/inf2.70170 by Hanyang University Library, Wiley Online Library on [08/11/2026]. See the Terms and Conditions (https://onlinelibrary.wiley.com/terms-and-conditions) on Wiley Online Library for rules of use; OA articles are governed by the applicable Creative Commons License

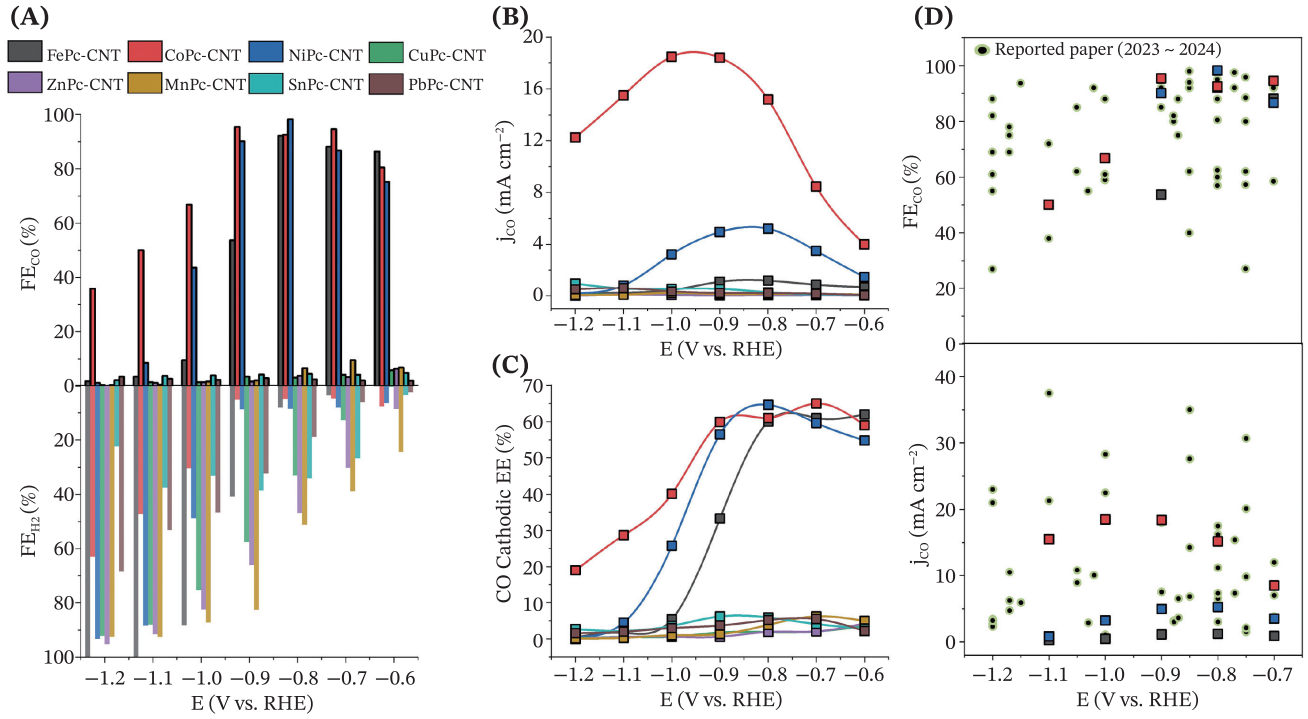

FIGURE 3 CO_2RR performance. (A) FE_{CO} and FE_{H_2} of MPc-CNTs at various applied voltages in CO_2-saturated 0.5 M $KHCO_3$ (pH = 7.23). (B) Potential-dependent CO partial current density and (C) CO cathodic energy efficiency of MPc-CNTs for CO_2RR. Experimental setup: A customized H-cell system with a catalyst loading of 1 mg cm^{-2}, an electrode area of 1 × 2 cm^2, and a geometric active area of 1 × 1 cm^2. The CO_2 flow rate was maintained at 20 mL min^{-1}. (D) Comparison of CO_2-to-CO electrocatalysts, based on 50 studies published between 2023 and 2024, identified using the keyword "electrochemical CO_2 reduction reaction" in the Web of Science database (Table S6).

systems, except for SnPc and PbPc, which exhibited longer distances of 4.69 and 4.90 Å, respectively (Table S4). While most MPc molecules adopted a square-planar geometry with D_{4h} symmetry, SnPc and PbPc exhibited a distinct nonplanar "shuttlecock" structure with C_{4v} symmetry (Figure S17). For these nonplanar species, two adsorption orientations were considered: metal-up and metal-down. DFT calculations showed that the metal-up configuration was more stable (Figure S18). To further assess the electronic influence of the CNT support, Bader charge and density of states (DOS) analyses were conducted. The Bader analysis revealed minimal changes in the charges of the metal centers across all MPc-CNT systems upon CNT introduction (Table S5). In contrast, the DOS results showed a noticeable reduction in the bandgap following CNT integration, indicating enhanced electronic interactions and more efficient charge transfer between the MPc molecules and the CNT support (Figure S19).[22,23] These changes likely contribute to the improved catalytic activity observed experimentally. Importantly, the oxidation state of the metal remained nearly unchanged, suggesting that the CNT primarily acts as an electronic conductor rather than altering the intrinsic electronic structure of the MPc.

2.2 | CO_2RR performance of MPc-CNTs

Electrochemical CO_2 conversion is a sustainable strategy that utilizes electrical energy to reduce atmospheric CO_2 levels.[24] This process plays a crucial role in advancing a carbon-neutral economy while enabling the transformation of CO_2 into high-value carbon products through proton-coupled electron transfer (PCET) mechanisms.[25] Single-centered MPc catalysts have attracted significant attention in catalysis research due to their remarkable ability to selectively and efficiently reduce CO_2 to carbon monoxide (CO), formate, and methanol (CH_3OH).

We evaluated the CO_2RR performance of eight fabricated MPc-CNT catalysts using chronoamperometric measurements over 1200 s in an H-cell system. The system was configured with a CO_2 flow rate of 20 mL min^{-1} and a 0.5 M $KHCO_3$ electrolyte to facilitate gas product analysis under CO_2RR conditions (Figure S20). Interestingly, CoPc-CNT not only exhibited superior CO_2 conversion performance over a broad potential range (−0.6 to −0.9 V vs. RHE) but also demonstrated a significantly higher CO partial current density (j_{CO}) compared to the other MPc-CNTs (Figure 3A,B). As depicted in Figure 3C, FePc-CNT, NiPc-CNT, and CoPc-CNT attained a CO

25673165, 2026, 10, Downloaded from https://onlinelibrary.wiley.com/doi/10.1002/inf2.70170 by Hanyang University Library, Wiley Online Library on [08/11/2026]. See the Terms and Conditions (https://onlinelibrary.wiley.com/terms-and-conditions) on Wiley Online Library for rules of use; OA articles are governed by the applicable Creative Commons License

cathodic energy efficiency exceeding 62%, indicating their exceptional capacity to convert electrical energy into CO_2 reduction products, a critical parameter for sustainability assessment. The electrochemical properties of these catalysts—including cyclic voltammetry (CV), TOF, electrochemical surface area (ECSA), and electrochemical impedance spectroscopy (EIS)—are presented in Figures S21–S24. We conducted an extended durability assessment of these catalysts and confirmed their stability over 8 h (Figure S25). At −0.9 V versus RHE, CoPc-CNT maintained a current density of ∼27.4 mA cm^{-2} and preserved the molecularly dispersed nature of the CoPc species (Figure S26). NiPc-CNT and FePc-CNT demonstrated exceptional stability at −0.8 V versus RHE, with an FE_{CO} decline of less than 5% and stable current densities. Furthermore, we assessed the relationship between fabrication cost and catalytic efficiency for CO_2RR using MPc-CNTs (Figure S27). A detailed cost analysis was performed to estimate the total expenses associated with fabricating a 1×2 cm^2 electrode (Supporting Information Note 2). The catalytic efficiency of MPc-CNTs was then compared to that of a conventional Ag foil electrode (Figure S28). As a result, FePc-CNT, NiPc-CNT, and CoPc-CNT exhibited remarkable price-to-performance improvements compared to commercial Ag foil at −0.8 V versus RHE, with enhancements of 63.34, 275.4, and 798.53-fold, respectively. Quantitative analysis of liquid-phase products revealed the characteristic CO_2RR selectivity trends of the examined MPc-CNT catalysts. CoPc-CNT generated less than 10% CH_3OH, whereas SnPc-CNT produced approximately 34% formate, as verified by nuclear magnetic resonance (NMR) spectroscopy (Figure S29). A comparison of the MPc-CNTs with 50 recently reported catalysts (2023–2024) further highlights their CO_2RR performance (Figure 3D). Furthermore, we implemented a catholyte-free MEA reactor featuring a zero-gap electrolyzer, which enabled higher current densities and larger electrodes (5 cm^2). When FePc-CNT and NiPc-CNT were incorporated as catalysts on the gas diffusion electrode (GDE) in the MEA reactor, H_2 generation became dominant at higher applied voltages (Figure S30). In stark contrast, CoPc-CNT exhibited an exceptional FE_{CO} of 99.2%, even under a constant current of 1000 mA. However, under ampere-level operation, the MEA system experienced severe carbonate precipitation at the GDE–membrane interface (Figure S31). This accumulation substantially restricted CO_2 transport to the MPc-CNT catalysts, triggering a rapid collapse in CO_2RR selectivity and a shift toward HER-dominant behavior. The resulting heterogeneous carbonate layer further induced pronounced current redistribution and short-circuit–like conductive pathways, collectively lowering the operating cell voltage. In conclusion, suppressing carbonate formation by implementing acidic proton-conducting environments or optimizing ion-transport management is critical for achieving stable, high-current CO_2 electrolysis. Details of the MEA configuration are provided in Supporting Information Note 3, and the experimental setups for both the H-cell and MEA electrolyzer are depicted in Figure S32.

2.3 | HER performance of MPc-CNTs

Given its high energy density and environmentally friendly nature, green H_2 is a promising alternative energy carrier.[26] Electrochemical water splitting powered by renewable energy offers an efficient and sustainable route for H_2 production.[27,28] Pt-based electrocatalysts are widely regarded for their superior performance in the HER, primarily due to their ability to facilitate rapid electron transfer, which efficiently drives the Volmer–Heyrovsky or Volmer–Tafel mechanisms.[29] Additionally, their optimal H adsorption free energy aligns with the Sabatier principle, ensuring a balanced adsorption–desorption process.[30] However, the high cost and scarcity of Pt necessitate the development of more economically viable and sustainable alternatives. In response to this challenge, we introduce eight MPc-CNTs as advanced electrocatalysts for H_2 generation, presenting a promising alternative to noble-metals-based catalysts.

The HER performance of the eight synthesized electrocatalysts was evaluated in a 0.5 M H_2SO_4 acidic electrolyte using a three-electrode setup. A 10 μL aliquot of MPc-CNT ink was drop-cast onto a glassy carbon electrode (GCE, *d*: 3 mm). To assess HER activity, the Tafel slope and overpotential were derived from polarization curves obtained through stabilized linear sweep voltammetry (LSV) measurements (Figure 4A,B). The Tafel slope, a key parameter reflecting the kinetic characteristics of the electrode reaction, indicated that MPc-CNTs predominantly followed the Volmer–Heyrovsky mechanism, in contrast to noble-metal catalysts. Among the MPc-CNTs, CoPc-CNT demonstrated a significantly lower overpotential and Tafel slope compared to previously reported CoPc (η_{10}: ∼497 mV, Tafel slope: 137 mV dec^{-1}).[31] In addition, CoPc-CNT and MnPc-CNT exhibited high TOFs, facilitating rapid HER kinetics and elevating overall electrode performance (Figure 4C). This enhanced activity may be attributed to improved electron-transfer efficiency. Electrochemical characterization of the MPc-CNTs, including EIS and durability tests, was performed (Figures S33 and S34). PdPc-CNT was additionally evaluated for HER activity and showed a Tafel slope of 96 mV dec^{-1} and an η_{10} of 163 mV, confirming its superior catalytic efficiency among the

25673165, 2026, 10, Downloaded from https://onlinelibrary.wiley.com/doi/10.1002/inf2.70170 by Hanyang University Library, Wiley Online Library on [08/11/2026]. See the Terms and Conditions (https://onlinelibrary.wiley.com/terms-and-conditions) on Wiley Online Library for rules of use; OA articles are governed by the applicable Creative Commons License

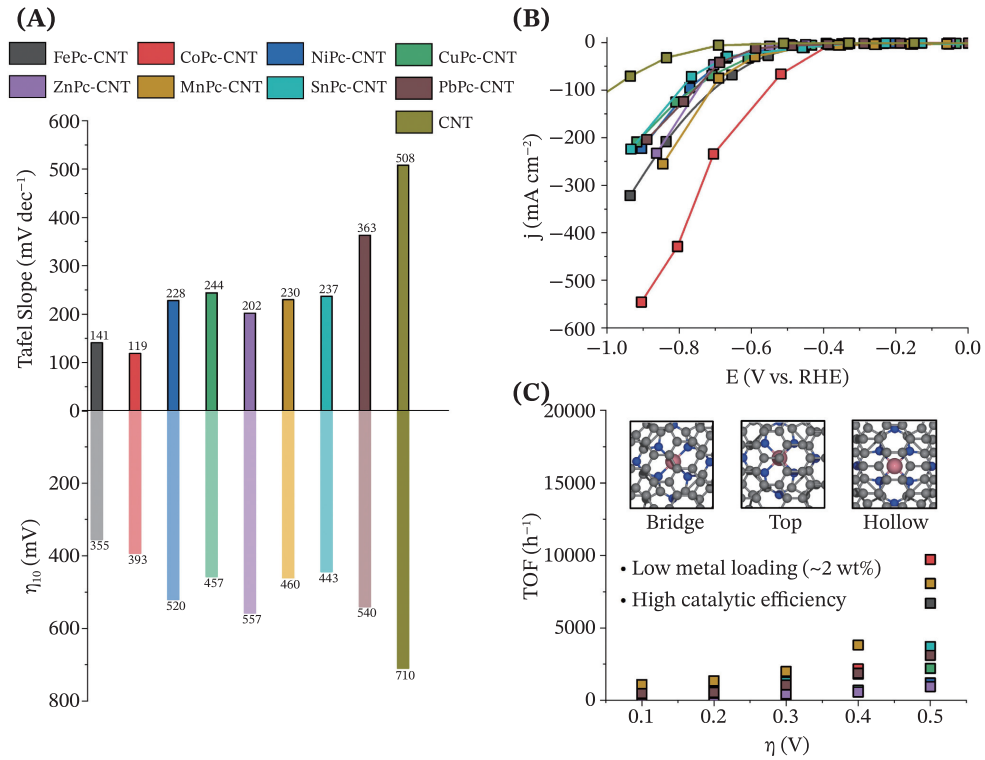

FIGURE 4 HER performance. (A) Tafel plots and the corresponding overpotentials at η_{10} for CNT and MPc-CNTs in acidic HER conditions. (B) Polarization curves (non-iR corrected). (C) TOF values of MPc-CNTs compared with those of pristine CNTs. TOF calculations were based on the precise metal weight percentage determined via ICP-MS measurements (Table S2). The inset depicts three thermodynamically favorable geometries of the central metal atom in MPc under electrochemical conditions, among which the bridge configuration was generally found to be the most stable. The experimental setup consisted of a customized H-cell system with a 0.5 M H_2SO_4 electrolyte (pH = 0), an electrode diameter of 3 mm, and a graphite rod as the counter electrode.

MPc-CNTs (Figure S35). However, its higher cost compared to other MPc-CNTs underscores the need for further investigation (Figure S36). To enhance the feasibility of H_2 production, we employed two strategies: (1) integrating a practical AEMWE device and (2) utilizing an alkaline electrolyte. The AEMWE system used a CoPc-CNT/Pt-coated carbon paper electrode (5 cm^2) as the cathode and stainless-steel gauze (SUS gz, 6.5 cm^2) as the anode. A significant increase in the current density was observed compared to electrodes lacking CoPc-CNT deposition (Figure S37). Moreover, at 80°C and 1 bar in 1 M KOH, current densities of 1 A cm^{-2} at 2.2 V and 2 A cm^{-2} at 2.5 V were achieved. Detailed configurations of the AEMWE device are provided in Supporting Information Note 4, and a digital photograph of the HER system is shown in Figure S38. To assess the performance stability, the long-term durability of CoPc-CNT was evaluated when used as the cathode in the AEMWE electrolyzer. Initial stability testing under high-current-density operation at 2 A cm^{-2} for 32 h demonstrated stable performance with no detectable changes in the local atomic environment, as confirmed by EXAFS analysis (Figure S39). To extend this evaluation to long-term operation, the catalyst–electrode interface was reinforced by increasing the Nafion solution content. As a result, the catalyst exhibited stable operation for 155 h at 1 A cm^{-2} under room-temperature conditions (Figure S40). Compared with previously reported catalysts, CoPc-CNT exhibited markedly enhanced HER performance (Figure S41).

2.4 | NRR performance of MPc-CNTs

The electrochemical conversion of N_2 to NH_3 has garnered significant attention as a sustainable alternative to the conventional Haber–Bosch (H–B) process.[32] The latter is an energy-intensive method that operates under high pressure and temperature, resulting in considerable energy consumption and CO_2 emissions.[33] In contrast, electrochemical NRR offers a promising route for NH_3 synthesis under ambient conditions, utilizing readily available N_2 and water. Recently, metallophthalocyanine-based catalysts have emerged as highly effective candidates for NRR due to their exceptional N_2 fixation capabilities, high NH_3 selectivity, and outstanding stability.[34] In this section, we assess the

25673165, 2026, 10, Downloaded from https://onlinelibrary.wiley.com/doi/10.1002/inf2.70170 by Hanyang University Library, Wiley Online Library on [08/11/2026]. See the Terms and Conditions (https://onlinelibrary.wiley.com/terms-and-conditions) on Wiley Online Library for rules of use; OA articles are governed by the applicable Creative Commons License

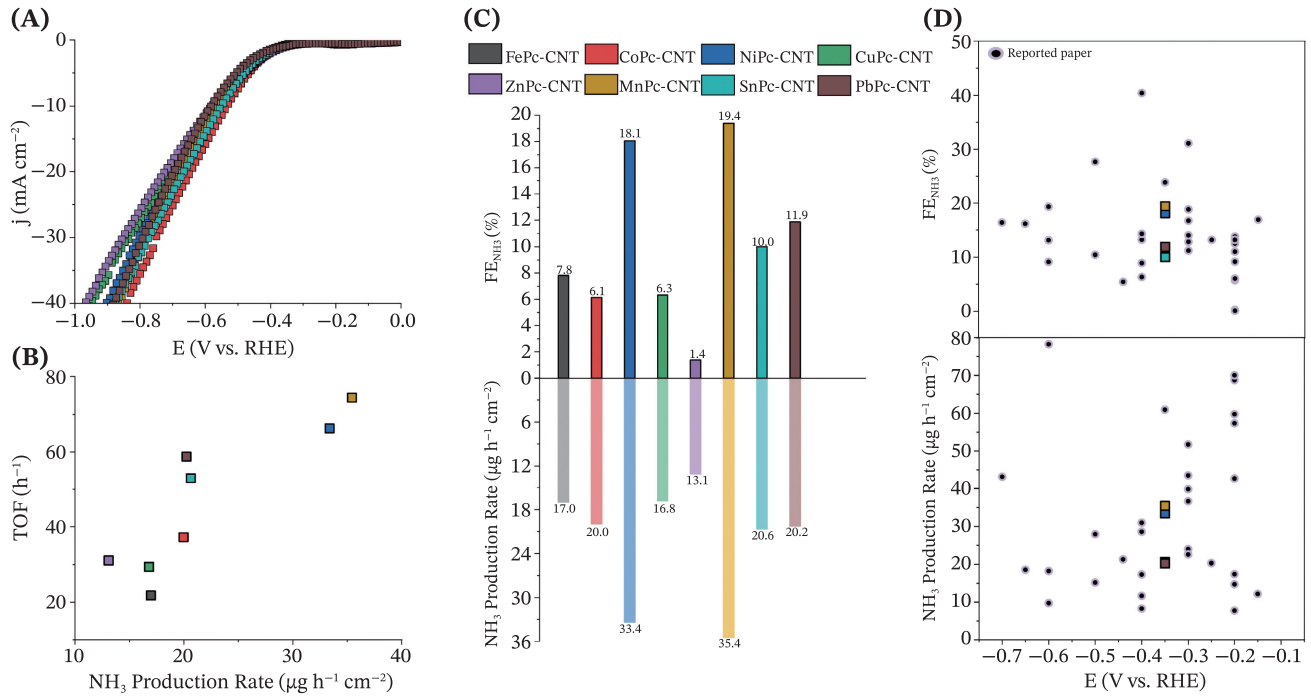

FIGURE 5 NRR performance. (A) LSV curves of MPc-CNTs in N_2-saturated 0.05 M H_2SO_4 (pH = 1.0). (B) TOF values and NH_3 production rates. The TOF calculation, based on ICP-MS measurements (Table S2). (C) FE_{NH_3} and NH_3 production rates at −0.35 V versus RHE. The produced NH_3 was quantified using the modified indophenol blue method. The experimental setup included a single-cell system with a catalyst loading of 0.5 mg cm^{-2}, an electrode area of 1 × 1 cm^2, and an N_2 gas flow rate of 30 mL min^{-1}. (D) Comparison of N_2-to-NH_3 conversion electrocatalysts based on 30 studies identified using the keyword "electrochemical nitrogen reduction reaction" from the Web of Science database (Table S7).

NRR performance of eight distinct MPc-CNT catalysts to identify the most efficient candidates, providing critical insights into the catalyst design and optimization for future research.

The electrochemical NRR performance of eight types of MPc-CNTs was evaluated in a 0.05 M H_2SO_4 acidic electrolyte under continuous N_2 purging in a single-cell configuration. LSV curves for MPc-CNTs were recorded from the open-circuit voltage (OCV) to −1.0 V versus RHE, revealing a comparable onset potential of approximately −0.35 V versus RHE (Figure 5A). The NRR experimental setup is detailed in Figure S42. To characterize the NRR activity, chronoamperometric measurements were conducted at a constant potential of −0.35 V versus RHE for 2 h (Figure S43). The produced NH_3 was quantified using the indophenol blue method, as outlined in Figure S44. Further electrochemical investigations, including LSV curve comparisons under Ar and N_2 environments and ECSA analysis of MPc-CNT electrodes, are provided in Figures S45 and S46. Strikingly, MnPc-CNT exhibited the highest TOF of 14.9 h^{-1} among the MPc-CNTs, highlighting its superior catalytic activity (Figure 5B). Among the tested MPc-CNTs, NiPc-CNT and MnPc-CNT demonstrated the highest NRR performance, achieving FE_{NH_3} values of 18.1% and 19.4% and NH_3 production rates of 33.4 and 35.4 μg h^{-1} cm^{-2}, respectively (Figure 5C). These results were further contextualized by comparison with 30 previously reported catalysts, underscoring their enhanced efficiency (Figure 5D). Extended electrochemical characterization at −0.4 and − 0.45 V versus RHE confirmed the exceptional NRR activity of NiPc-CNT and MnPc-CNT (Figures S47 and S48). The FE of NH_3 for both catalysts decreased at more negative potentials, while NH_3 production rates peaked at −0.4 V versus RHE before significantly dropping at −0.45 V versus RHE, due to the dominance of hydrogen evolution. Long-term stability tests conducted at −0.35 V versus RHE over 8 consecutive hours demonstrated that NiPc-CNT maintained a stable FE_{NH_3} and production rate, whereas MnPc-CNT exhibited a gradual decline in catalytic activity over time (Figures S49 and S50). To verify the nitrogen source of NH_3 and to exclude potential contamination and false-positive signals, $^{15}N_2$ isotope labeling experiments were conducted. The produced $^{15}NH_3$ was quantified by ^{1}H NMR spectroscopy using NiPc-CNT and MnPc-CNT, which exhibited the highest Faradaic efficiencies among the MPc-CNT catalysts. After electrolysis, the characteristic doublet peak corresponding to $^{15}NH_4^+$ was clearly observed, confirming that NH_3 originated from NRR (Figure S51).

25673165, 2026, 10, Downloaded from https://onlinelibrary.wiley.com/doi/10.1002/inf2.70170 by Hanyang University Library, Wiley Online Library on [08/11/2026]. See the Terms and Conditions (https://onlinelibrary.wiley.com/terms-and-conditions) on Wiley Online Library for rules of use; OA articles are governed by the applicable Creative Commons License

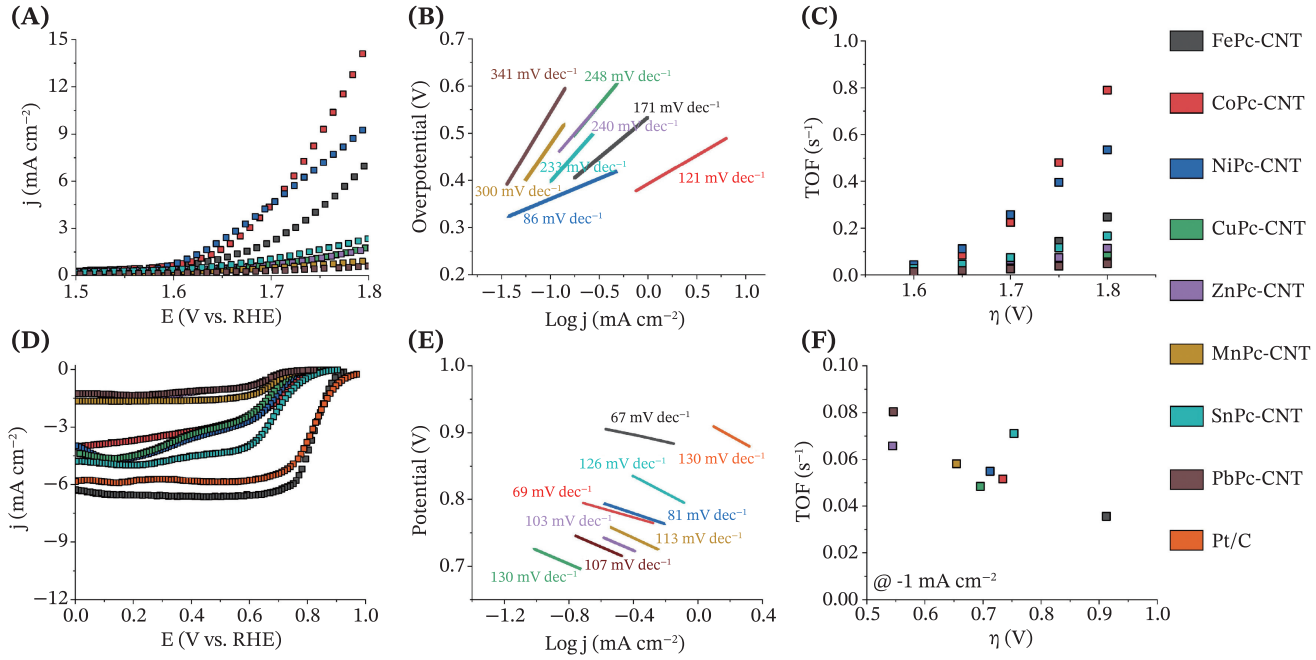

FIGURE 6 OER and ORR performances. (A) LSV curves of eight different MPc-CNTs. (B) Tafel plots corresponding to the OER LSV curves. (C) TOF values of MPc-CNTs measured at potentials ranging from 1.6 V to 1.8 V versus RHE. (D) LSV curves of eight different MPc-CNTs and commercial Pt/C. (E) Tafel plots corresponding to the LSV curves for the ORR. (F) TOF values of MPc-CNTs at -1 mA cm^{-2}. To compare MPc-CNTs, the TOF values for the OER and ORR were calculated at a current density of 1 mA cm^{-2}. Experimental setup: RDE system with a rotation rate of 1600 rpm, GCE area = 0.1965 cm^2, electrolyte: 1 M KOH for OER and 0.1 M KOH for ORR.

2.5 | OER/ORR performance of MPc-CNTs

In industrial-scale electrochemical water splitting systems, overall system efficiency is primarily dictated by the OER at the anode, which counterbalances the HER at the cathode.[35] This highlights the need to develop energy-efficient OER catalysts to enhance system performance.[36] Although noble-metal-based catalysts such as IrO_2 and RuO_2 exhibit exceptional OER activity, their high costs and limited natural abundance significantly hinder their large-scale applicability. Similarly, the ORR, which is crucial for the efficient operation of fuel cells and metal-air batteries, is limited by the scarcity and limited long-term stability of noble metals used in electrodes (e.g., Pt).[37] These limitations highlight the urgent need to optimize alternative electrocatalysts. In this study, we investigated MPc-CNT composites as potential electrocatalysts for both the OER and ORR, aiming to identify promising non-noble metal-based candidates and provide valuable insights for future research.

Both OER and ORR activities of MPc-CNTs were evaluated using a rotating disk electrode (RDE) setup at 1600 rpm in Ar-purged 1 M KOH and O_2-saturated 0.1 M KOH, respectively. MPc-CNTs were deposited onto a GCE (d: 5 mm) via drop-casting at a loading of 0.2 mg cm^{-2}. A detailed digital photograph of the OER/ORR setup is shown in Figure S52. To assess OER performance, LSV curves were recorded from the OCV to 1.8 V versus RHE and compared with those of RuO_2 (Figure 6A and Figure S53). All MPc-CNTs exhibited overpotentials exceeding 0.35 V relative to the theoretical OER potential (1.23 V vs. RHE), suggesting inferior catalytic activity compared with RuO_2. Among the MPc-CNTs, CoPc-CNT demonstrated the highest performance, with a Tafel slope of 121 mV dec^{-1} and the greatest TOF (Figure 6B,C). The augmented activity of CoPc-CNT may be attributed to its efficient electron transfer capabilities and enhanced oxygen formation kinetics, as reflected in the TOF results. For the ORR, LSV curves were recorded from the OCV to 0 V versus RHE and compared with those of Pt/C (Figure 6D). Among the tested catalysts, FePc-CNT exhibited the highest activity, characterized by a Tafel slope of 67 mV dec^{-1} and a high TOF, surpassing not only other MPc-CNT catalysts but also Pt/C (Figure 6E,F). These findings align with previous studies identifying Fe-based phthalocyanines as highly effective ORR electrocatalysts, underscoring their potential for energy conversion applications. The present ORR results primarily provide a comparative evaluation of catalytic activity among the MPc-CNTs, while detailed pathway analysis would require additional rotating ring-disk electrode (RRDE)-based investigations.

25673165, 2026, 10, Downloaded from https://onlinelibrary.wiley.com/doi/10.1002/inf2.70170 by Hanyang University Library, Wiley Online Library on [08/11/2026]. See the Terms and Conditions (https://onlinelibrary.wiley.com/terms-and-conditions) on Wiley Online Library for rules of use; OA articles are governed by the applicable Creative Commons License

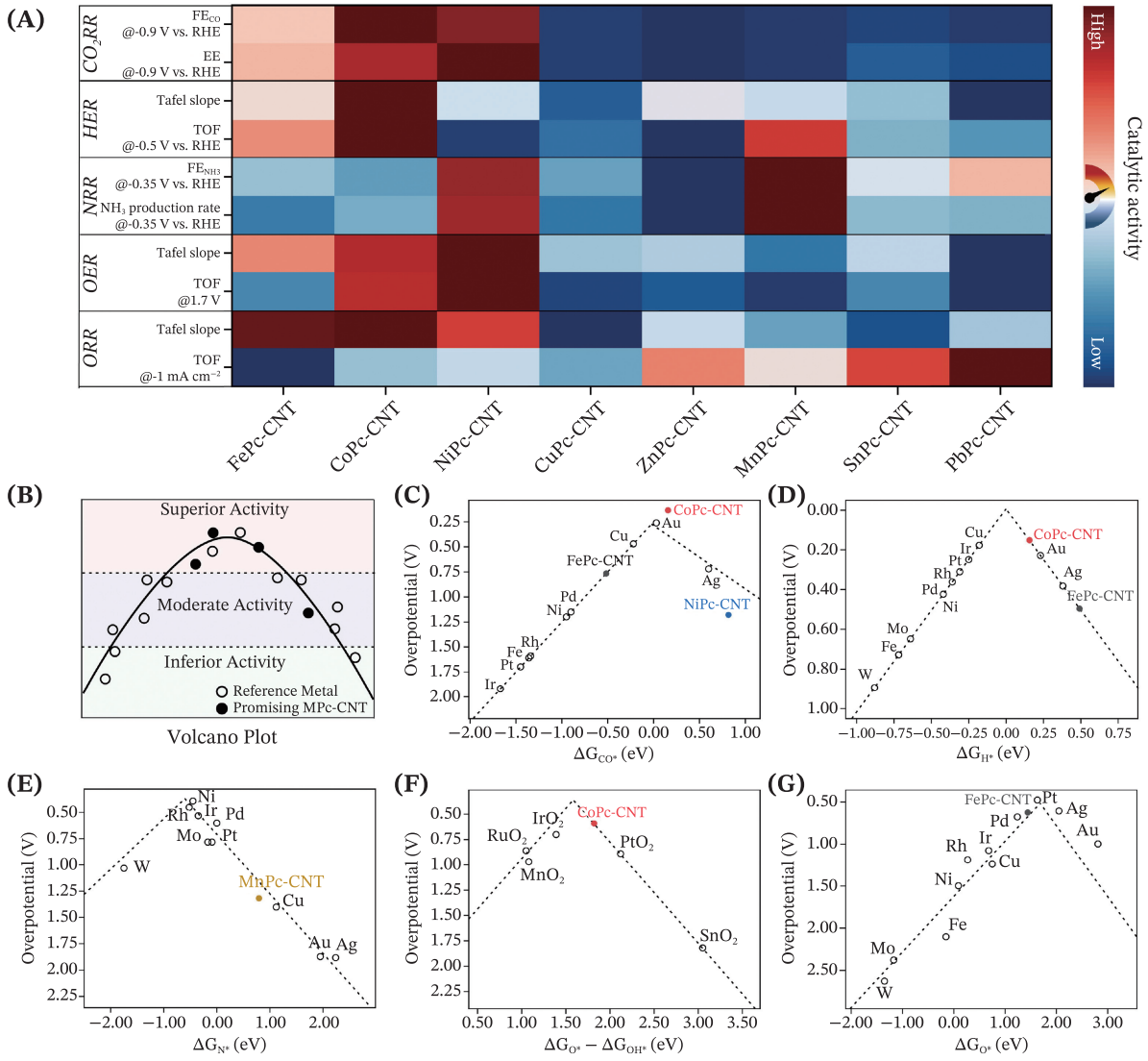

FIGURE 7 Experimentally derived heat map and theoretical volcano plots of MPc-CNTs versus conventional metal catalysts. (A) A heat map illustrating the catalytic activity of MPc-CNTs across five electrochemical energy conversion processes is presented. The x-axis represents different MPc-CNTs, while the y-axis denotes key factors influencing each of the five electrochemical energy conversion applications. Regions in dark red indicate the highest catalytic activity, while dark blue signifies the lowest activity. White regions represent intermediate catalytic performance. The values of all factors were normalized within predefined ranges determined based on *Pearson correlation coefficients*. (B) Schematic illustration of the workflow for electrocatalytic evaluation. (C) CO_2RR activity trend as a function of ΔG_{CO*}. (D) HER activity trend as a function of ΔG_{H*}. (E) NRR activity trend as a function of ΔG_{N*}. (F) OER volcano plot as a function of ΔG_{O*}–ΔG_{OH*}. (G) ORR volcano plot as a function of ΔG_{O*}.

2.6 | MPc-CNTs versus the rest: Theoretical investigations

The experimentally derived heat maps (Figure 7A), constructed using reaction-specific electrochemical platforms, were intended to capture overarching activity trends rather than provide absolute comparisons under identical conditions. Guided by these experimental insights, DFT calculations were performed to systematically evaluate the catalytic performance of MPc electrocatalysts across five electrochemical reactions. The Gibbs free energies (ΔG) of key reaction intermediates were calculated to construct descriptor-based volcano plots, benchmarking MPc catalysts against well-established reference metal surfaces and providing comparative insights into their catalytic behavior (Figure 7B). For CO_2RR, the adsorption free energy of CO (ΔG_{CO*}) was used as the descriptor,[38] with (211) transition metal surfaces serving as references.[39] CoPc-CNT was located near the top of the CO_2RR volcano plot, indicating its exceptional catalytic activity consistent with experimental results (Figure 7C). For HER, the hydrogen adsorption

25673165, 2026, 10, Downloaded from https://onlinelibrary.wiley.com/doi/10.1002/inf2.70170 by Hanyang University Library, Wiley Online Library on [08/11/2026]. See the Terms and Conditions (https://onlinelibrary.wiley.com/terms-and-conditions) on Wiley Online Library for rules of use; OA articles are governed by the applicable Creative Commons License

free energy (ΔG_{H^*}) was selected as the descriptor.[40] CoPc-CNT was positioned near the top of the HER volcano plot, demonstrating near-optimal catalytic performance in agreement with experiments (Figure 7D). While MnPc-CNT displayed moderate performance toward NRR, it was positioned relatively far from the volcano peak derived from ΔG_{N^*} values using (111) transition metal surfaces as references. Nevertheless, it outperformed noble metals such as Au and Ag, suggesting that targeted optimization strategies may further enhance its activity (Figure 7E).[41] For OER, the volcano plot was constructed using ΔG_{O^*}–ΔG_{OH^*} as the descriptor with (110) facets of rutile metal oxides as references.[42] CoPc-CNT exhibited a low theoretical overpotential and was located near the top of the volcano plot, indicating strong performance as a non-precious OER catalyst (Figure 7F). For ORR, ΔG_{O^*} was used as the descriptor and (111) FCC metal surfaces served as references.[43] FePc-CNT displayed catalytic performance comparable to Pt (Figure 7G). This result highlights its potential as a cost-effective alternative to noble-metal ORR catalysts. Beyond standard volcano plot analyses, dataset-driven approaches can provide broader insights, such as the identification of universal descriptors for catalyst screening. However, benchmarking MPc-CNT catalysts against bulk reference metals presents a challenge due to their fundamentally different electronic structures and bonding characteristics. Specifically, reference metals exhibit broad, continuous d-bands, whereas MPc-CNT catalysts contain isolated metal centers that give rise to discrete, peak-like d-states. Consequently, while electronic-structure descriptors like the d-band center are effective for interpreting trends within a single material class, applying them uniformly across both bulk metals and MPc-CNTs is not physically rigorous. Furthermore, the MPc-CNT library encompasses both 3d transition-metal and post-transition-metal centers, which possess substantially different valence electronic structures. Therefore, we identified the adsorption free energies of key reaction intermediates as the most robust and unified descriptors for this diverse library. Unlike electronic metrics, these thermodynamic descriptors provide a transferable basis for comparison across different catalyst classes. Regardless of the underlying electronic differences, intermediate adsorption free energies offer a direct and comparable indicator of catalytic activity. Overall, these descriptor-based volcano analyses provide a quantitative benchmarking and interpretative framework that reveals the distinct catalytic behaviors of MPc-CNT catalysts across diverse electrochemical reactions, establishing a systematic energetics-based reference for comparing catalytic performance across different material classes.

2.7 | Design considerations for optimal metal loading and scalability

The catalytic performance and practical applicability of MPc-CNT electrodes are critically governed by metal loading, which mediates the balance between the density of electrochemically accessible active sites and their effective utilization under realistic operating conditions. To systematically investigate the effect of metal loading, MPc-CNT catalysts were synthesized using half, optimal, and double precursor amounts, denoted as MPc-CNT-1, MPc-CNT-2, and MPc-CNT-3, respectively, focusing on the most active MPc catalysts for each electrochemical reaction, as identified from the volcano plot analysis. The influence of metal loading on catalytic activity was comprehensively evaluated (Figures S54–S57). In addition, the scalability of the optimized loading was validated through a tenfold scale-up synthesis under controlled precursor conditions (Table S8), yielding materials that retained their intrinsic activity and selectivity compared to laboratory-scale samples (Figure S58).

3 | CONCLUSIONS

To tackle the pressing environmental crisis confronting humanity, we carried out a study integrating eight metallophthalocyanine-based catalysts into five cutting-edge electrochemical energy conversion processes, constructing a robust electrocatalyst library to systematically explore catalysts for these diverse processes. This approach accelerates the identification of optimal catalysts and elucidation of key performance trends, enabling improved efficiency and sustainability. By addressing simplified synthesis, reproducibility, cost-effectiveness, and scalability, this study lays the groundwork for the industrial implementation of MPc-based electrocatalysts and provides theoretical insights to guide their further development.

ACKNOWLEDGMENTS

This research was supported in part by the NRF funded by the Korean government (RS-2025-00558945). Seoin Back acknowledges the support from the National Research Foundation of Korea (NRF) grant funded by the Korea government (MSIT) (RS-2025-02214715) and generous supercomputing time from KISTI.

CONFLICT OF INTEREST STATEMENT

The authors declare no conflict of interest.

25673165, 2026, 10, Downloaded from https://onlinelibrary.wiley.com/doi/10.1002/inf2.70170 by Hanyang University Library, Wiley Online Library on [08/11/2026]. See the Terms and Conditions (https://onlinelibrary.wiley.com/terms-and-conditions) on Wiley Online Library for rules of use; OA articles are governed by the applicable Creative Commons License

DATA AVAILABILITY STATEMENT

The data that supports the findings of this study are available in the Supporting Information of this article.

ORCID

Sang Hyun Ahn https://orcid.org/0000-0001-8906-5908
Youn Jeong Jang https://orcid.org/0000-0002-2400-0473
Soo Young Kim https://orcid.org/0000-0002-0685-7991

REFERENCES

1. Grant D, Hansen T, Jorgenson A, Longhofer W. A worldwide analysis of stranded fossil fuel assets' impact on power plants' CO_2 emissions. *Nat Commun*. 2024;15(1):7517.
2. Dunant C, Hafez H, March ATM, et al. Timely deployment of best-in-class technologies to enable development and decarbonise construction. *Nat Commun*. 2026;17:799.
3. Ye J, Dimitratos N, Rossi LM, Thonemann N, Beale AM, Wojcieszak R. Hydrogenation of CO_2 for sustainable fuel and chemical production. *Science*. 2025;387(6737):943.
4. Corzo D, Rosas-Villalva D, Amruth C, et al. High-performing organic electronics using terpene green solvents from renewable feedstock. *Nat Energy*. 2023;8(1):62-73.
5. Noufal M, Santiago ARP, Tolba SA, et al. Co–Cu bimetallic metal organic framework catalyst outperforms the Pt/C benchmark for oxygen reduction. *J Am Chem Soc*. 2021;143(10):4064-4073.
6. Zeng Z, Chang K-C, Kubal J, Markovic NM, Greeley J. Stabilization of ultrathin (hydroxy)oxide films on transition metal substrates for electrochemical energy conversion. *Nat Energy*. 2017;2(6):17070.
7. Wang T, Miao L, Zheng S, et al. Interfacial engineering of Ni_3N/Mo_2N heterojunctions for urea-assisted hydrogen evolution reaction. *ACS Catal*. 2023;13(7):4091-4100.
8. Li J, Zhu Q, Chang A, et al. Molecular-scale CO spillover on a dual-site electrocatalyst enhances methanol production from CO_2 reduction. *Nat Nanotechnol*. 2025;20(4):515-522.
9. He H, Zhu Q-Q, Yan Y, et al. Metal–organic framework supported Au nanoparticles with organosilicone coating for high-efficiency electrocatalytic N_2 reduction to NH_3. *Appl Catal B-Environ*. 2022;302:120840.
10. Liu S, Li C, Zachman MJ, et al. Atomically dispersed iron sites with a nitrogen–carbon coating as highly active and durable oxygen reduction catalysts for fuel cells. *Nat Energy*. 2022;7(7):652-663.
11. Cui P, Zhao L, Long Y, Dai L, Hu C. Carbon-based Electrocatalysts for acidic oxygen reduction reaction. *Angew Chem Int Ed*. 2023;62(14):e202218269.
12. Ding J, Yang HB, Ma XL, et al. A tin-based tandem electrocatalyst for CO_2 reduction to ethanol with 80% selectivity. *Nat Energy*. 2023;8(12):1386-1394.
13. Yi JD, Si D-H, Xie R, et al. Conductive two-dimensional Phthalocyanine-based metal–organic framework nanosheets for efficient electroreduction of CO_2. *Angew Chem Int Ed*. 2021;60(31):17108-17114.
14. Zhang X, Wang Y, Gu M, et al. Molecular engineering of dispersed nickel phthalocyanines on carbon nanotubes for selective CO_2 reduction. *Nat Energy*. 2020;5(9):684-692.
15. Yang HB, Hung S-F, Liu S, et al. Atomically dispersed Ni(i) as the active site for electrochemical CO_2 reduction. *Nat Energy*. 2018;3(2):140-147.
16. Adalder A, Paul S, Barman N, et al. Controlling the metal–ligand coordination environment of manganese Phthalocyanine in 1D–2D heterostructure for enhancing nitrate reduction to ammonia. *ACS Catal*. 2023;13(20):13516-13527.
17. Mukherjee J, Paul S, Adalder A, et al. Understanding the site-selective Electrocatalytic Co-reduction mechanism for green urea synthesis using copper Phthalocyanine nanotubes. *Adv Funct Mater*. 2022;32(31):2200882.
18. Su J, Musgrave CB III, Song Y, et al. Strain enhances the activity of molecular electrocatalysts via carbon nanotube supports. *Nat Catal*. 2023;6(9):818-828.
19. Feng S, Wang X, Cheng D, et al. Stabilizing $*CO_2$ intermediates at the acidic Interface using molecularly dispersed cobalt Phthalocyanine as catalysts for CO_2 reduction. *Angew Chem Int Ed*. 2024;63:e202317942.
20. Mei B, Mao J, Liang Z, et al. Reversible angle distortion-dependent electrochemical CO_2 reduction on cobalt Phthalocyanine. *J Am Chem Soc*. 2025;147(7):5819-5827.
21. Ma J, Cho JH, Lee C, et al. Unraveling the harmonious coexistence of ruthenium states on a self-standing electrode for enhanced hydrogen evolution reaction. *Energy Environ Mater*. 2024;7:e12766.
22. Kim K, Lee J, Park OK, et al. Geometric tuning of single-atom FeN_4 sites via edge-generation enhances multi-enzymatic properties. *Adv Mater*. 2023;35(19):2207666.
23. Kim K, Lee J, Park OK, et al. Enhanced Cuproptosis via metabolic reprogramming using copper-delivering Co–N–C single-atom Nanozyme. *ACS Nano*. 2025;19(24):21969-21982.
24. Wang S, Li F, Zhao J, et al. Manipulating C-C coupling pathway in electrochemical CO_2 reduction for selective ethylene and ethanol production over single-atom alloy catalyst. *Nat Commun*. 2024;15(1):10247.
25. Cho JH, Lee C, Hong SH, et al. Transition metal ion doping on ZIF-8 enhances the electrochemical CO_2 reduction reaction. *Adv Mater*. 2023;35:2208224.
26. Zhou S, Cao W, Shang L, et al. Facilitating alkaline hydrogen evolution kinetics via interfacial modulation of hydrogen-bond networks by porous amine cages. *Nat Commun*. 2025;16(1):1849.
27. Sun H, Xu X, Kim H, Jung W, Zhou W, Shao Z. Electrochemical water splitting: bridging the gaps between fundamental research and industrial applications. *Energy Environ Mater*. 2023;6:e12441.
28. Li Z, Wang Y, Liu H, et al. Electroreduction-driven distorted nanotwins activate pure Cu for efficient hydrogen evolution. *Nat Mater*. 2025;24(3):424-432.
29. Fan Y, Zhang S, Ye X, et al. Unique single-phase electrocatalyst for excellent overall water splitting facilitated by multi-atom synergistic effects. *InfoMat*. 2025;7(10):e70053.
30. Chen ZW, Li J, Ou P, et al. Unusual Sabatier principle on high entropy alloy catalysts for hydrogen evolution reactions. *Nat Commun*. 2024;15(1):359.
31. Balogun SA, Thole D, Masekela D, Modibane KD. Cobalt Phthalocyanine-based photo/Electrocatalysts for hydrogen evolution reaction. *Adv Energy Sustainability Res*. 2024;5:2400169.

25673165, 2026, 10, Downloaded from https://onlinelibrary.wiley.com/doi/10.1002/inf2.70170 by Hanyang University Library, Wiley Online Library on [08/11/2026]. See the Terms and Conditions (https://onlinelibrary.wiley.com/terms-and-conditions) on Wiley Online Library for rules of use; OA articles are governed by the applicable Creative Commons License

32. Winter LR, Chen JG. N_2 fixation by plasma-activated processes. *Joule*. 2021;5(2):300-315.
33. Ren Y, Yu C, Tan X, et al. Strategies to activate inert nitrogen molecules for efficient ammonia electrosynthesis: current status, challenges, and perspectives. *Energ Environ Sci*. 2022;15(7):2776-2805.
34. Murmu S, Paul S, Santra A, Robert M, Ghorai UK. Graphene wrapped nickel phthalocyanine nanohybrid: efficient electrocatalyst for nitrogen reduction reaction. *Catal Today*. 2023;423:113938.
35. Huang J, Clark AH, Hales N, et al. Oxidation of interfacial cobalt controls the pH dependence of the oxygen evolution reaction. *Nat Chem*. 2025;17(6):856-864.
36. Rong C, Huang X, Arandiyan H, Shao Z, Wang Y, Chen Y. Advances in oxygen evolution reaction Electrocatalysts via direct oxygen–oxygen radical coupling pathway. *Adv Mater*. 2025;37(9):2416362.
37. Varga T, Vásárhelyi L, Ballai G, et al. Noble-metal-free iron nitride/nitrogen-doped graphene composite for the oxygen reduction reaction. *ACS Omega*. 2019;4(1):130-139.
38. Cho JH, Ma J, Lee C, et al. Crystallographically vacancy-induced MOF nanosheet as rational single-atom support for accelerating CO_2 electroreduction to CO. *Carbon Energy*. 2024;6(8):e510.
39. Hansen HA, Varley JB, Peterson AA, Nørskov JK. Understanding trends in the Electrocatalytic activity of metals and enzymes for CO_2 reduction to CO. *J Phys Chem Lett*. 2013;4(3):388-392.
40. Nørskov JK, Bligaard T, Logadottir A, et al. Trends in the exchange current for hydrogen evolution. *J Electrochem Soc*. 2005;152(3):J23.
41. Montoya JH, Tsai C, Vojvodic A, Nørskov JK. The challenge of electrochemical ammonia synthesis: a new perspective on the role of nitrogen scaling relations. *ChemSusChem*. 2015;8(13):2180-2186.
42. Yeom K, Jo J, Shin H, et al. Unraveling surface reconstruction during oxygen evolution reaction on the defined spinel oxide surface. *Adv Funct Mater*. 2024;34(36):2401095.
43. Nørskov JK, Rossmeisl J, Logadottir A, et al. Origin of the Overpotential for oxygen reduction at a fuel-cell cathode. *J Phys Chem B*. 2004;108(46):17886-17892.

SUPPORTING INFORMATION

Additional supporting information can be found online in the Supporting Information section at the end of this article.

How to cite this article: Cho JH, Moon YH, Yu G, et al. Building a library of electrocatalysts based on single-centered metallophthalocyanines. *InfoMat*. 2026;8(10):e70170. doi:10.1002/inf2.70170

25673165, 2026, 10, Downloaded from https://onlinelibrary.wiley.com/doi/10.1002/inf2.70170 by Hanyang University Library, Wiley Online Library on [08/11/2026]. See the Terms and Conditions (https://onlinelibrary.wiley.com/terms-and-conditions) on Wiley Online Library for rules of use; OA articles are governed by the applicable Creative Commons License